Acceleration Feedback Control for Atmospheric Reduced Gravity Flights

Mohammed Nasser Aldosari *
King Abdullah University of Science and Technology, Thuwal, Makkah Province,23955-6900, Saudi Arabia

Yi-Hsuan Chen†
University of Maryland, College Park, MD, 20740, USA

Adeel Akhtar‡
New Jersey Institute of Technology, Newark, NJ, 07102, USA

Eric Feron§
King Abdullah University of Science and Technology, Thuwal, Makkah Province,23955-6900, Saudi Arabia

The simulation of reduced gravity environments plays a significant role in advancing scientific research and the ongoing pursuit of space exploration. While various platforms for microgravity experiments exist, the demand for an accessible, cost-efficient, and flexible solution remains. Aircraft stands out as a promising platform, offering a more economical and readily available option for reduced-gravity research compared to other platforms. This study aims to develop control laws for an autopilot system, enabling precise and reliable aircraft control for a range of reduced gravity levels. The control architecture comprises two specialized controllers, each dedicated to managing acceleration along the tangential and normal axes of the body frame, using the aircraft's engine thrust and elevator. Building upon prior work, the tangential acceleration controller has three integral actions to enable it to reject the unmeasured drag force efficiently. On the other hand, the accelerometer is positioned in the cockpit to effectively avoid the non-minimum phase behavior of the transfer function from elevator deflection to the normal acceleration of the CG of the airplane. Detailed MATLAB simulation results indicate that the proposed control law allows the system to achieve and maintain any reduced gravity level, including zero gravity, with duration and quality that significantly exceeds the expected benchmarks.

Nomenclature

α	=	angle of attack, rad
a_x, a_z	=	tangential and normal accelerations of the airplane CG, m/s^2
a_{px}, a_{pz}	=	proper acceleration components in x- and z-axes, m/s^2
a_{kx}, a_{kz}	=	cockpit acceleration components in x- and z-axes, m/s^2
AR	=	wing aspect ratio
C_{px}, C_{pz}	=	tangential and normal acceleration controllers
C_m, C_D, C_L	=	moment, drag, and lift coefficients
$\bar{c}$	=	mean aerodynamic chord, m
D	=	drag force, N
δ_e	=	elevator deflection, rad
e	=	Oswald efficiency factor
F_G	=	gravitational force, N
$\mathcal{F}_B$	=	body-fixed frame (x^B, z^B)

*Ph.D. candidate, Mechanical Engineering, mohammed.aldosari@kaust.edu.sa.
†Ph.D. student, Department of Aerospace Engineering, yhchen91@umd.edu.
‡Assistant Professor, Department of Mechanical and Industrial Engineering, adeel.akhtar@njit.edu
§Professor, Electrical and Computer Engineering, eric.feron@kaust.edu.sa, AIAA fellow.

$\mathcal{F}_E$	=	Earth-fixed inertial frame (x^E, z^E)
$\mathcal{F}_S$	=	stability frame (x^S, z^S)
g	=	acceleration due to gravity, m/s^2
G	=	gravitational constant, $N \cdot m^2/kg^2$
γ	=	flight path angle, rad
$H(s)$	=	transfer function
I_y	=	moment of inertia about y-axis, $kg \cdot m^2$
L	=	lift force, N
M_y	=	moment about the y-axis, $N \cdot m$
m	=	mass of the aircraft, kg
$\boldsymbol{\omega}$	=	angular velocity, rad/s
S	=	wing reference area, m^2
Q	=	dynamic pressure, N/m^2
q	=	pitch rate, rad/s
V	=	airspeed, m/s
W	=	weight, N
T	=	thrust, N
θ	=	pitch angle, rad
u	=	velocity component of the CG along the x^B axis, m/s
w	=	velocity component of the CG along the z^B axis, m/s
X	=	non-gravitational forces along the x^B axis, N
Z	=	non-gravitational forces along the z^B axis, N
λ	=	terrestrial longitude
ϕ	=	geodetic latitude
V_N	=	geographic system north component of velocity over Earth
V_E	=	geographic system east component of velocity over Earth
$\mathbb{R}$	=	the set of real numbers
$\mathbb{R}^n$	=	the n-dimensional Euclidean space
$\times$	=	the standard cross product in $\mathbb{R}^3$
$:=$	=	equal by definition
$\sum$	=	summation symbol
Subscripts		
cg	=	center of gravity
k	=	the point k, which is located in the cockpit and aligned with x^B-axis
p	=	proper or local acceleration

I. Introduction

Gravity is one of the universe's fundamental forces, along with electromagnetic, strong, and weak interactions. It is the force of attraction that exists between any two masses. Gravity is essential for life on Earth, governing everything from atmospheric stability and climate to biological functions and biodiversity through its influence on the hydrological cycle and tides. In the larger context of the universe, gravity is responsible for forming celestial bodies, their orbital movements, and the very structure of space-time itself.

While gravity's fundamental role in shaping our world and universe is indisputable, the ability to manipulate or simulate its effects marks a significant step forward in our quest for scientific understanding and technological advancement. Creating reduced gravity conditions on Earth or within the atmosphere is important for advancing various scientific and engineering endeavors. These reduced gravity environments serve as a testing ground for hypotheses and technologies that will be deployed in outer space. By replicating these conditions, researchers can study the physiological responses of humans and other organisms to long-term exposure to low-gravity environments, thereby informing space medicine and long-duration space travel. It also allows engineers to rigorously test spacecraft, robotic equipment, and other technologies in conditions that mimic their eventual operational settings. Furthermore, these simulations can facilitate experiments in fundamental physics [1], combustion [2], medical [3], and physiological [4] sciences that are not possible in Earth's gravity, thereby opening new avenues for scientific discovery [5].

Reduced gravity refers to conditions where the force of gravity is less than what is experienced on Earth. Reduced

gravity can range from microgravity, a condition close to weightlessness, through the low levels experienced on the Moon (about 1/6th of Earth's gravity) to higher levels like those on Mars (about 3/8th of Earth's gravity). According to Newton's law of universal gravitation, every object attracts every other object in the universe with a force that is proportional to the product of their masses and inversely proportional to the square of the distance between their centers. i.e. $F_G = Gm_1m_2/r^2$, where F_G is the gravitational force, m_1 and m_2 are the masses of the objects interacting, r is the distance between the centers of the objects, and G is the gravitational constant. The nullification of gravitational force would require either one of the objects to have zero mass or an infinite separation between them, both of which are physically unattainable scenarios. Therefore, completely nullifying gravitational force is not possible. However, it is possible to simulate the microgravity environments by following the trajectory of a free-falling object, where the free-falling object enters the weightlessness state (a condition when the apparent weight of the body is zero). For an object to be in a perfect free-falling condition, all forces acting on it must be nullified except the gravity force, which causes the free-fall motion. From the viewpoint of an observer on the Earth's (inertial) reference frame, the object falls with a constant acceleration. While in the body reference frame, the object's apparent weight is zero, although its mass does not change [5–7].

In a gravitational field like Earth, an object experiences weightlessness, or zero apparent weight, when in a state of free fall. Under such conditions, all external forces acting upon the object cancel out, leaving only its weight as the acting force. In other words, the object must be falling under the influence of gravity alone, with no other forces—such as air resistance. Furthermore, the apparent weight of an object can be manipulated by adjusting the reaction force exerted upon it by the surface on which it stands. For instance, an increased normal (reaction) force from the surface can make the object feel like it is experiencing a stronger gravitational field than Earth.

Microgravity can be achieved using a variety of platforms such as drop facilities, sounding rockets, orbiting spacecraft, or aircraft [7]. Table 1 provides a comparison in terms of the microgravity duration and levels that each platform can achieve. Aircraft, which are the focus of this study, are used to achieve microgravity conditions for several seconds, depending on their capabilities, by flying following the trajectory of a free-falling object. Different types of aircraft can be used to perform atmospheric reduced-gravity flights, that include airliners [8], general aviation airplanes [9], gliders [10], and fixed-wing and multi-rotors unmanned aerial vehicles (UAV) [11, 12]. Each of these aircraft categories is capable of performing the parabolic flight maneuver to create microgravity conditions for a certain duration and level of microgravity.

Table 1 Microgravity Platforms [13]

Platform	Duration	G-level
Drop Towers	2-9 sec	$10^{-2} - 10^{-5}g$
Aircraft	25 sec	$10^{-2} - 10^{-3}g$
Balloon-drop	60 sec	$10^{-2} - 10^{-3}g$
Sounding rockets	6 min	$10^{-3} - 10^{-4}g$
Space shuttle	$> 9 - 11$ days	$10^{-3} - 10^{-5}g$
Space station	$>$ months	$10^{-5} - 10^{-6}g$

Aircraft, when used as a reduced gravity platform, offers several advantages over the aforementioned methods, including drop towers and space-based facilities. Specifically, aircraft are highly versatile and can be adapted to a wide range of experimental requirements, making them suitable for diverse scientific studies. They provide larger space and payload capacity compared to drop towers, allowing for more complex and expansive experiments. Unlike space-based platforms such as the International Space Station (ISS), which require extensive planning and substantial costs for access, aircraft can be more readily available and cost-effective, making them accessible to a broader range of researchers and students. Another significant advantage of using aircraft for reduced gravity research is the ability to conduct multiple experiments in a single flight. This contrasts with drop towers, which typically allow only one experiment per drop. Aircraft can also offer longer durations of microgravity, up to 30 seconds in some cases, compared to only a few seconds provided by drop towers. Furthermore, by adjusting the flight profile, aircraft can be used to achieve various gravity levels, from martian and lunar gravity to zero gravity. This flexibility is not typically available with other platforms. In addition, repeated aircraft use for experiments can lead to iterative refinements and modifications based on previous results, fostering a more dynamic and responsive research process. Overall, the use of aircraft as microgravity platforms

combines accessibility, versatility, and cost-effectiveness with the ability to serve a wide array of research needs, making them a valuable tool in the realm of reduced gravity research.

However, manually performing the atmospheric microgravity maneuvers requires highly skilled pilots to achieve the desired precision and time of the microgravity condition. For example, to perform the maneuver using a jet airliner, like Boeing 727 [14] or Airbus A310 [15], three highly-trained pilots are needed in the cockpit to control pitch, roll, and thrust independently. That introduces an element of human error and variability, potentially affecting the consistency and repeatability of the experiments, apart from the availability of highly-trained pilots for each experimental run. Therefore, the goal of this study is to design an efficient flight controller that can autonomously conduct precise reduced-gravity flights. This controller aims to automate the complex process of achieving and maintaining reduced gravity conditions, thereby reducing reliance on expert pilots and opening up new possibilities for more consistent, frequent, and accessible reduced gravity research.

A. Literature Review

Numerous research studies have been undertaken to develop flight controllers enabling aircraft to execute microgravity flights autonomously; e.g., see [16–19] and the references therein. Broadly, the existing body of work in flight controller design can be categorized into two primary methodologies: trajectory tracking and direct acceleration control.

The trajectory tracking approach is based on calculating a specific flight trajectory that an aircraft must follow to achieve reduced gravity conditions. This is determined by taking into account the aircraft's initial velocity and path angle. In 1996, Amato et al. proposed a control system that combines two control actions: a feedforward control for optimal trajectory tracking in the absence of external disturbances and a gain-scheduled output feedback control to counteract misalignments due to environmental disturbances like wind gusts. However, this approach necessitates the measurement of all states, which may not be practical, especially during a zero-gravity maneuver where the entire operation unfolds within a few seconds [16]. Similarly, Hathaway et al. developed an automatic controller for microgravity UAVs to follow a ballistic trajectory. A MATLAB simulator is developed to test the controller, and hardware-in-the-loop (HIL) tests are conducted using X-plane software. However, the study acknowledges the challenges in dealing with the effects of gusts and atmospheric unsteadiness on smaller aircraft, requiring more responsive control systems [17]. Chen et al. propose a novel control logic inspired by drag-free satellites, utilizing a proof-mass-tracking approach. This control strategy uses a triple-integral control architecture, which is capable of maintaining zero gravity conditions without precise information about drag. However, this approach is limited to zero gravity maneuvers and can not be extended to other reduced gravity flights [18].

The direct acceleration control method utilizes an accelerometer to measure the aircraft's acceleration, enabling the system to detect and correct deviations from predefined target values effectively. In 2011, Hofmeister and Blum engineered a fixed-wing UAV designed for executing parabolic flights. The UAV employs accelerometers to accurately measure its vertical acceleration, which is then compared to a predetermined set point. To effectively reduce acceleration along the longitudinal axis, the system utilizes a pre-control mechanism based on the measured flight speed for real-time drag estimation and compensation. However, the UAV is too sensitive to wind variations due to its size, making it not suited for vibration-sensitive experiments [11]. Similarly, Higashino and Kozai introduce a 6-degree-of-freedom simulation model to examine the feasibility of achieving a microgravity environment using two types of acceleration feedback systems: feedback in body axes and wind axes. The control system, leveraging PID controllers, manipulates the throttle and elevator to control acceleration components in these axes, with the control gains determined to ensure system stability, optimal response time, and damping characteristics. Flight tests were also conducted using the acceleration component feedback in body axes, which, despite the limited adjustment of control gains, achieved a minimum G-level of approximately $0.15g$. Although this level may not be sufficient for practical applications of microgravity, it demonstrates the feasibility of achieving such an environment using small UAVs [19]. Additionally, using a PID controller alone is insufficient for rejecting the drag force, as explored in the studies [20] and [18], which emphasize the need for control strategies with triple integral actions.

Moreover, some studies investigate improving and optimizing aircraft design to improve aircraft response and ability to reject any disturbances. For example, Kraeger's study explores using a free-wing UAV for microgravity experimentation. The UAV is designed with a free-wing mechanism, where the wing can rotate about an axis slightly ahead of the aerodynamic center. This design allows for more adaptive and responsive control of the aircraft's attitude. The study concludes that using a free-wing UAV with PI controllers shows promise for accurately flying partial-gravity trajectories and managing gust responses. However, the study acknowledges the need for further optimization of the UAV design to enhance its performance in microgravity research. Moreover, conducting flight tests is necessary to

validate the practical feasibility and effectiveness of the free-wing concept in real-world scenarios [21].

B. Contributions of the Study

This study makes several contributions to the field of flight controller design for reduced gravity flights, which includes

- employing acceleration as the primary feedback, allowing for maneuvers to rely mainly on a single, reliable sensor;
- strategically placing the accelerometer in the cockpit, addressing and mitigating non-minimum phase behavior in the control system;
- achieving any level of reduced gravity under ideal weather conditions utilizing the proposed flight control law;
- ensuring simulation fidelity to real-life scenarios by considering thrust and elevator initiation and servo dynamics, closely mirroring actual flight conditions.

II. Flight Maneuver

For an object to be in a weightlessness (or free-fall) situation, it must be subject to no force except the gravitational force. We consider an airplane flying in a straight and level flight. The forces acting on it are its weight, lift, drag, and thrust. For the aircraft to be in free fall, all forces acting on it must be nullified except its weight. Haber et al. [22], in 1950, found that an airplane can simulate the motion of a free-falling object by following a nearly parabolic trajectory.

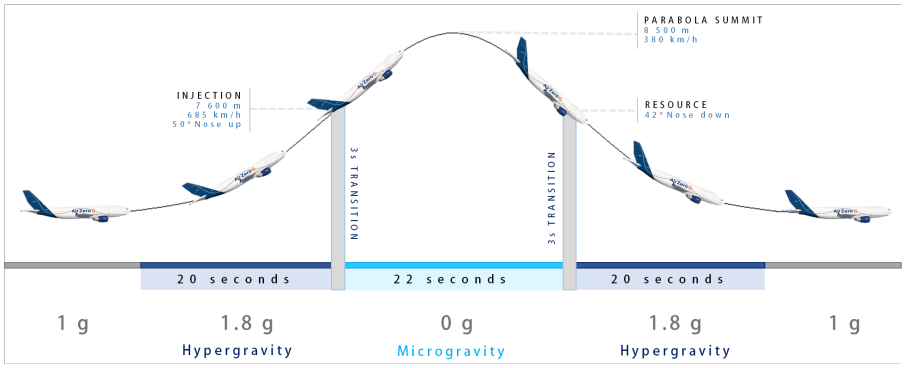

Fig. 1 The different gravity phases during a parabolic flight [23].

The parabolic flight maneuver can be divided into four phases: speed-up, pull-up, reduced gravity, and pull-out phases; see Figure 1 for details. **Speed-up phase**: At the beginning of the maneuver, the airplane accelerates at a steady, leveled flight to reach a desirable speed. **Pull-up phase**: The aircraft then climbs with a full thrust to keep the same airspeed, and passengers and objects in the aircraft experience hyper-gravity levels of $1.5 - 1.8g$. **Reduced gravity phase**: After reaching the planned altitude and at $45 - 50^\circ$ pitching angle, the reduced gravity segment is initiated by reducing the angle of attack α (which causes a reduction in lift force) and decreasing the thrust to a level just sufficient to compensate the effect of air drag. In this phase, the airplane's motion approximates that of a free-falling object rather than of an aerodynamic vehicle. **Pull-out phase**: After approximately 20-25 seconds of reduced gravity phase, when the airplane reaches the end of the parabola with a nose pitched down at $45 - 50^\circ$, the airplane's nose pulled up, and the thrust is increased to decrease its downward speed and recover to the to steady level flight. Passengers and objects again experience hyper-gravity levels of $1.5 - 1.8g$ during the pull-out phase. Then, the cycle can be restarted [24].

III. Airplane Model

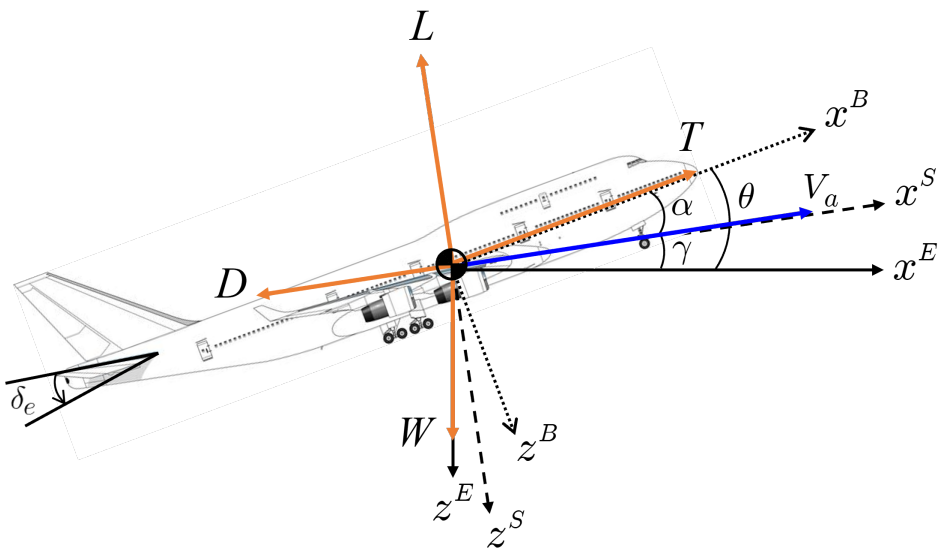

Fig. 2 Free body diagram of an airplane, illustrating the primary reference frames and forces acting on the aircraft during flight.

We make two primary assumptions to create a manageable yet insightful analytical framework for our study. First, we assume that the engine thrust is perfectly aligned with the body's x-axis, effectively eliminating any moment generated by the thrust force. Second, we confine our study to a 2D plane, focusing solely on longitudinal dynamics.

Consider a typical airplane, see Figure 2, along with forces acting on the airplane and the three reference frames, namely inertial reference frame $\mathcal{F}_E = (x^E, z^E)$, body reference frame $\mathcal{F}_B = (x^B, z^B)$, and stability reference frame $\mathcal{F}_S = (x^S, z^S)$. The origins of both $\mathcal{F}_B$ and $\mathcal{F}_S$ are located at the aircraft's center of gravity. For xz-planar motion and by Newton's second law of motion, the summation of forces (ΣF_x and ΣF_z) and the summation of moments about the y-axis (ΣM_y) are given by

$$\Sigma F_x = ma_x, \quad \Sigma F_z = ma_z, \quad \Sigma M_y = I_y \dot{q}, \tag{1}$$

where $m \in \mathbb{R}$ is the mass of the aircraft, $a_x \in \mathbb{R}$ and $a_z \in \mathbb{R}$ are the tangential and normal accelerations, respectively, $I_y \in \mathbb{R}$ represents the moment of inertia about y-axis, and $\dot{q} \in \mathbb{R}$, i.e., time derivative of q, represents the rate of change of the pitch rate. The forces acting on the airplane can be expressed along the body axis as

$$\Sigma F_x = T - D\cos\alpha + L\sin\alpha - W\sin\theta, \tag{2}$$

$$\Sigma F_z = -D\sin\alpha - L\cos\alpha + W\cos\theta, \tag{3}$$

where the scalar quantities T, D, L and W are thrust, drag, lift, and weight forces, respectively, and $\alpha \in \mathbb{R}$ and $\theta \in \mathbb{R}$ are the angle of attack and the pitch angle, respectively. The moment, drag force, and lift force can be defined as

$$M_y = C_m QS, \tag{4}$$

$$D = C_D QS, \tag{5}$$

$$L = C_L QS, \tag{6}$$

where $S \in \mathbb{R}$ is the wing reference area, $Q \in \mathbb{R}$ is the dynamic pressure, the scalars C_m, C_D, and C_L are the moment, drag, and lift coefficients respectively. These coefficients can be defined as

$$C_m = C_{m_0} + C_{m_\alpha}\alpha + C_{m_q}\frac{q\bar{c}}{2V} + C_{m_{\delta_e}}\delta_e, \tag{7}$$

$$C_L = C_{L_0} + C_{L_\alpha}\alpha + C_{L_q}\frac{q\bar{c}}{2V} + C_{L_{\delta_e}}\delta_e, \tag{8}$$

$$C_D = C_{D_0} + \frac{C_L^2}{\pi ARe}, \tag{9}$$

where AR is the Aspect Ratio, $e \in \mathbb{R}$ is the Oswald efficiency factor, which is typically less than 1, and $\bar{c} \in \mathbb{R}$, $V \in \mathbb{R}$, and $\delta_e \in \mathbb{R}$ are the wing mean cord length, the airspeed, and the elevator deflection, respectively. Moreover, the scalars $C_{m_0}, C_{m_\alpha}, C_{m_q}, C_{m_{\delta_e}}, C_{L_0}, C_{L_\alpha}, C_{L_q}, C_{L_{\delta_e}}$, and C_{D_0} are longitudinal stability derivatives. Values of the longitudinal derivatives of a few airplane models can be found in [25].

Now, let us consider the right-hand side of equations (1); Based on the Transport Theorem, the acceleration $\mathbf{a} \in \mathbb{R}^3$ and moment $\mathbf{M} \in \mathbb{R}^3$ of the airplane at its CG in the inertial reference frame $\mathcal{F}_E$ can be described as

$$\mathbf{a} = \dot{\mathbf{V}} + \boldsymbol{\omega} \times \mathbf{V}, \tag{10}$$

$$\mathbf{M} = \dot{\mathbf{H}} + \boldsymbol{\omega} \times \mathbf{H}, \tag{11}$$

where the symbols $\mathbf{V} \in \mathbb{R}^3$ and $\boldsymbol{\omega} \in \mathbb{R}^3$ are linear and angular velocities along the body reference frame, respectively, and $\mathbf{H} \in \mathbb{R}^3$ is the angular momentum about the CG.
For xz-planar motion, we can rewrite the above equations as

$$\begin{bmatrix} a_x \\ a_y \\ a_z \end{bmatrix} = \begin{bmatrix} \dot{u} \\ 0 \\ \dot{w} \end{bmatrix} + \begin{bmatrix} 0 \\ q \\ 0 \end{bmatrix} \times \begin{bmatrix} u \\ 0 \\ w \end{bmatrix}, \tag{12}$$

$$\begin{bmatrix} M_x \\ M_y \\ M_z \end{bmatrix} = \begin{bmatrix} 0 \\ \dot{H}_y \\ 0 \end{bmatrix} + \begin{bmatrix} 0 \\ q \\ 0 \end{bmatrix} \times \begin{bmatrix} 0 \\ H_y \\ 0 \end{bmatrix}, \tag{13}$$

where $u \in \mathbb{R}$ and $w \in \mathbb{R}$ are the body-axis forward and vertical speeds and $q \in \mathbb{R}$ is the pitch rate. Hence, the scalar equations of the acceleration components are

$$a_x = \dot{u} + qw, \tag{14}$$

$$a_z = \dot{w} - qu, \tag{15}$$

and the moment about the y-axis equation is

$$M_y = I_y \dot{q}. \tag{16}$$

Therefore, from equations (2),(3), (14), and (15), the nonlinear equations of motion that describe the longitudinal dynamics of an airplane can be defined as

$$m(\dot{u} + qw) = T - D\cos\alpha + L\sin\alpha - W\sin\theta, \tag{17}$$

$$m(\dot{w} - qu) = -D\sin\alpha - L\cos\alpha + W\cos\theta, \tag{18}$$

$$I_y \dot{q} = M_y. \tag{19}$$

Let the state space variables be defined as $\mathbf{X} := (u, w, q, \theta) \in \mathbb{R}^4$. By rearranging equations (17), (18),and (19), one can derive the differential equations that describe the changes in the prescribed state variables

$$\dot{u} = \frac{1}{m}[T - D\cos\alpha + L\sin\alpha - W\sin\theta - mqw], \tag{20}$$

$$\dot{w} = \frac{1}{m}[-D\sin\alpha - L\cos\alpha + W\cos\theta + mqu], \tag{21}$$

$$\dot{q} = M_y / I_y, \tag{22}$$

$$\dot{\theta} = q. \tag{23}$$

The forces acting on the aircraft, i.e., $\Sigma F \in \mathbb{R}^3$ can be divided into aerodynamic, gravitational, and thrust forces such that

$$\Sigma F = F_{\text{aerodynamic}} + F_{\text{gravitational}} + F_{\text{thrust}}.$$

Moreover, as discussed in Section I, the aerodynamic and thrust (i.e., the non-gravitational) forces must be canceled by each other for the airplane and its occupants to be in a perfect free-falling situation. From equations (17) and (18), the non-gravitational forces can be defined as

$$X = T - D\cos\alpha + L\sin\alpha = m(\dot{u} + qw) + mg\sin\theta, \tag{24}$$

$$Z = -D\sin\alpha - L\cos\alpha = m(\dot{w} - qu) - mg\cos\theta. \tag{25}$$

When equations (24) and (25) are divided by the mass of the aircraft, we get the equations of the *proper acceleration* of the aircraft, such as

$$a_{px} = \dot{u} + qw + g\sin\theta, \tag{26}$$
$$a_{pz} = \dot{w} - qu - g\cos\theta, \tag{27}$$

where the "proper acceleration" components in x^B- and z^B-axes are denoted as $a_{px} \in \mathbb{R}$ and $a_{pz} \in \mathbb{R}$.

The term "proper acceleration" refers to the acceleration experienced by an object from the perspective of an observer or an instrument fixed to the object itself. This type of acceleration is distinct from coordinate acceleration, which is measured in relation to a separate, external reference frame, like the Earth. Proper acceleration is what is directly felt by the occupants of the aircraft as a tangible force, and it is independent of gravitational acceleration. This is the acceleration that an accelerometer fixed to the aircraft would measure, as it provides a reading of the forces acting on the aircraft minus the effect of gravity. For example, consider a scenario where an airplane is taking off: as the engines increase thrust, the airplane accelerates along the runway, and the passengers inside feel the sensation of being pushed back into their seats. This sensation is the proper acceleration — it is the result of the net force acting on the airplane and its occupants. Similarly, during maneuvers like steep climbs, sharp turns, or rapid descents, the passengers would feel forces pushing them against their seats or pulling them away from them. These are all instances of proper acceleration. An accelerometer in the airplane would measure these changes, providing data on the intensity and direction of these forces. Hence, in zero-gravity conditions, the proper acceleration has to be zero, i.e.,

$$a_{px} = a_{pz} = 0, \tag{28}$$

and for the reduced gravity case, which is a more general case, some acceleration along the normal axis (z^B) is desired, i.e.,

$$a_{px} = 0, \tag{29}$$
$$a_{pz} = -\mu g, \tag{30}$$

where $0 \leq \mu \leq 1$.

IV. Problem Formulation

Given a Boeing B-747 airplane or a similar aircraft equipped with a typical IMU sensor placed in the cockpit, we aim to design two flight controllers. The goal of the first controller is to force the magnitude of the proper acceleration in the x^B-direction close to zero in some finite time t_s, i.e., $|a_{px}(t)| \to 0$ as $t \to t_s$. Typically, $t_s < 5$s. Moreover, the magnitude of the proper acceleration stays close to zero for some desired duration of reduced gravity T, which is approximately $25 - 30$ seconds. In other words,

$$|a_{px}(t)| < 0_\epsilon, \quad \text{for all } t \in [t_s, T],$$

where $0_\epsilon \in \mathbb{R}_{\geq 0}$ is less than $0.1 m/s^2$.

Similarly, the goal of the second controller is to force the magnitude of the proper acceleration in the z^B-direction close to a given reduced gravity level in some finite time t_s, i.e., $|a_{px}(t)| \to \mu g$ as $t \to t_s$ with $\mu \in [0, 1]$. Typically, $t_s < 5$s. Moreover, the magnitude of the proper acceleration stays close to the given reduced gravity for some desired duration of the reduced gravity duration T, which is approximately $25 - 30$ seconds. In other words,

$$|a_{pz}(t) - \mu g| < 0_\delta, \quad \text{for all } t \in [t_s, T],$$

where $0_\delta \in \mathbb{R}_{\geq 0}$ is less than $0.1 m/s^2$.

Informally and simply put, the goal is to design a controller that achieves a desired level of gravity with little settling time and little or no steady-state error.

V. Proposed Control Architecture

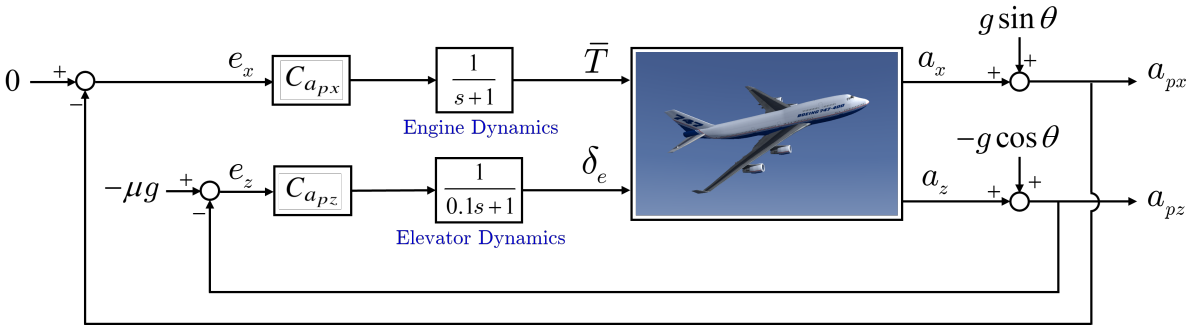

Fig. 3 Proposed control architecture block diagram

Our proposed control architecture consists of two specialized controllers, indicated by $C_{a_{px}} : \mathbb{R} \to \mathbb{R}$ and $C_{a_{pz}} : \mathbb{R} \to \mathbb{R}$ in Figure 3, each tasked with the precise regulation of proper acceleration along specific axes, integral to the successful simulation of reduced-gravity environments. The control input vector is defined as $\mathbf{U} := (\delta_e, \bar{T}) \in \mathbb{R}^2$, where δ_e and $\bar{T}$ are the elevator deflection and the normalized thrust ($\bar{T} := T/m$) respectively. The first controller $C_{a_{pz}}$, dedicated to managing acceleration along the z^B-axis, will utilize the airplane's elevator as its primary control mechanism. This system's design hinges on the real-time interpretation and response to data from onboard accelerometers, which will continuously monitor changes in vertical acceleration. Concurrently, the second controller $C_{a_{px}}$ is envisioned to govern the aircraft's acceleration along the x^B-axis, employing the engine's thrust as its main control variable. This controller's role is to maintain a steady forward motion, ensuring zero acceleration along the x^B-axis to preserve the integrity of the reduced-gravity conditions. This is achieved through precise thrust management, with accelerometers providing real-time feedback. Figure 3 illustrates the proposed control architecture. There is a separate loop for each controller. In each control loop, the difference between the desired and the actual accelerations is fed to the controller, which, by its role, will calculate the required action (thrust setting for x^B-axis accelerations and elevator deflection for z^B-axis accelerations) to minimize the error. However, the plant's output is the coordinate acceleration. Meanwhile, the accelerometer measures the proper acceleration, which is the coordinate acceleration minus the gravity component. Therefore, the gravity component is considered as a disturbance that has to be rejected by the proposed controller. To enhance the simulation's realism, servo dynamics are integrated to account for the elevator and jet engine response delays to flight controller commands. Moreover, the initial condition of input of $C_{a_{px}}$ is maximum thrust. That ensures a more accurate representation of real-world aircraft behavior.

VI. Normal Acceleration Control

In this section, we discuss the development of the normal acceleration controller. We start by linearizing the nonlinear longitudinal equations of motion (17-19) using the small disturbance theory, as discussed in [25]. To represent the system in the "standard" linear control system form, i.e., $\dot{\mathbf{X}} = \mathbf{AX} + \mathbf{BU}$, we compute $\mathbf{A}$ and $\mathbf{B}$ matrices as follows:

$$\mathbf{A} = \begin{bmatrix} X_u & X_w & 0 & -g\cos\theta_0 \\ Z_u & Z_w & u_0 & -g\sin\theta_0 \\ M_u + M_{\dot{w}} Z_u & M_w + M_{\dot{w}} Z_w & M_q + M_{\dot{w}} u_0 & 0 \\ 0 & 0 & 1 & 0 \end{bmatrix}, \tag{31}$$

$$\mathbf{B} = \begin{bmatrix} X_{\delta_e} & X_{\delta_T} \\ Z_{\delta_e} & Z_{\delta_T} \\ M_{\delta_e} + M_{\dot{w}} Z_{\delta_e} & M_{\delta_T} + M_{\dot{w}} Z_{\delta_T} \\ 0 & 0 \end{bmatrix}. \tag{32}$$

Since the goal is to get a desired acceleration along the z^B-axis, the obvious output of the system is the normal acceleration measured by an accelerometer placed at the center of gravity of the aircraft. However, with the deflection angle of the elevator used as a control input, the acceleration control system has *non-minimum phase* characteristics. Non-minimum phase behavior in a system refers to a phenomenon where the system's initial response to a control input is in the opposite direction of its steady-state response. The non-minimum phase poses significant challenges in control

system design, particularly in ensuring stability and managing transient responses, as it requires the control strategy to account for the initial counter-response before achieving the desired long-term behavior [26].

To demonstrate this non-minimum phase behavior, let us derive the transfer function from elevator to acceleration $H(s) = a_z/\delta_e$. As we discussed previously in Section V, the output of the plant is a_z, and the gravity component, i.e., $-g\cos\theta$ is considered as a disturbance added to the plant output. For simplification, we approximate the short-period mode of motion by assuming $\Delta u = 0$ and dropping the X-force equation. The short-period approximation is highly suitable for designing a controller for vertical acceleration in aircraft due to its focus on pitch dynamics, which are directly related to vertical acceleration through changes in the angle of attack and lift. This approximation, isolating high-frequency, short-term pitch and angle of attack dynamics from the lower-frequency, long-term phugoid mode, simplifies the complex longitudinal dynamics of aircraft into a second-order system, which is given as

$$\begin{bmatrix} \dot{w} \\ \dot{q} \end{bmatrix} = \begin{bmatrix} Z_w & u_0 \\ M_w + M_{\dot{w}} Z_w & M_q + M_{\dot{w}} u_0 \end{bmatrix} \begin{bmatrix} w \\ q \end{bmatrix} + \begin{bmatrix} Z_{\delta_e} \\ M_{\delta_e} + M_{\dot{w}} Z_{\delta_e} \end{bmatrix} \delta_e. \tag{33}$$

We define

$$\mathbf{A_z} := \begin{bmatrix} Z_w & u_0 \\ M_w + M_{\dot{w}} Z_w & M_q + M_{\dot{w}} u_0 \end{bmatrix}, \quad \text{and} \tag{34}$$

$$\mathbf{B_z} := \begin{bmatrix} Z_{\delta_e} \\ M_{\delta_e} + M_{\dot{w}} Z_{\delta_e} \end{bmatrix} \tag{35}$$

Next, consider equation (15) which is expressed as $a_z = \dot{w} - q u_0$. Using equation (33), we get

$$\dot{w} - q u_0 = \begin{bmatrix} Z_w & 0 \end{bmatrix} \begin{bmatrix} w \\ q \end{bmatrix} + \begin{bmatrix} Z_{\delta_e} \end{bmatrix} \delta_e.$$

Then, we define the output matrix $\mathbf{C_z}$ and the feedthrough matrix $\mathbf{D_z}$ as

$$\mathbf{C_z} := \begin{bmatrix} Z_w & 0 \end{bmatrix}, \tag{36}$$

$$\mathbf{D_z} := \begin{bmatrix} Z_{\delta_e} \end{bmatrix}. \tag{37}$$

Given $\mathbf{A_z}$, $\mathbf{B_z}$, $\mathbf{C_z}$, and $\mathbf{D_z}$, the transfer function $H_z(s)$ can be determined by using the following

$$H_z(s) = \mathbf{C_z}(s\mathbf{I} - \mathbf{A_z})^{-1}\mathbf{B_z} + \mathbf{D_z}. \tag{38}$$

For Boeing B-747 with $u_0 = 180 m/s$, the transfer function is

$$H_z(s) = \frac{(s + 9.237)(s - 7.475)}{s^2 + 2.893s + 5.729}.$$

Hence, $H_z(s)$ has a positive real zero, which implies the non-minimum phase behavior of the system.

A. Placing the accelerometer in the cockpit

As we discussed, using the vertical acceleration of the CG as the output variable leads to the formation of a non-minimum phase system characterized by inherent difficulties in achieving stable control. Specifically, when high gain is applied in an attempt to stabilize the system, it results in an unstable control response. Conversely, adopting a low control gain to mitigate this instability introduces performance inefficiencies, making it challenging to achieve the desired precision in control. This dilemma indicates that relying on CG acceleration feedback as the primary control mechanism is inherently suboptimal for our application. Consequently, this issue necessitates the exploration and identification of an alternative output variable for acceleration. This new variable must be conducive to creating a minimum phase system when paired with elevator deflection as the input. Such a system would inherently possess more favorable response characteristics, allowing for stable and efficient control. A potential alternative is the acceleration of a point ahead of the CG. By placing the accelerometer in a position ahead of the CG, such as the cockpit, the system will have a minimum phase behavior [18, 27].

The acceleration of an arbitrary point k in the airplane is calculated as

$$\mathbf{a_k} = \mathbf{a} + \dot{\boldsymbol{\omega}} \times \mathbf{r_{k|cg}} + \boldsymbol{\omega} \times (\boldsymbol{\omega} \times \mathbf{r_{k|cg}}), \tag{39}$$

where the notation $\mathbf{r_{k|cg}} \in \mathbb{R}^3$ represents the position vector from the center of gravity to the point k. We assume that both the CG and the point k lie on the body's x-axis, then $\mathbf{r_{k|cg}} = (d_{k|cg}, 0, 0)$. For xz-planar motion, we can write

$$\begin{bmatrix} a_{kx} \\ 0 \\ a_{kz} \end{bmatrix} = \begin{bmatrix} a_x \\ 0 \\ a_z \end{bmatrix} + \begin{bmatrix} 0 \\ \dot{q} \\ 0 \end{bmatrix} \times \begin{bmatrix} d_{k|cg} \\ 0 \\ 0 \end{bmatrix} + \begin{bmatrix} 0 \\ q \\ 0 \end{bmatrix} \times \begin{bmatrix} 0 \\ q \\ 0 \end{bmatrix} \times \begin{bmatrix} d_{k|cg} \\ 0 \\ 0 \end{bmatrix}.$$

The acceleration of the point k is expressed as

$$a_{kx} = \dot{u} + qw - d_{k|cg}q^2, \tag{40}$$
$$a_{kz} = \dot{w} - qu - d_{k|cg}\dot{q}. \tag{41}$$

Now, let us find the transfer function for the acceleration in the z-direction using the short-period approximation

$$a_{kz} = \dot{w} - qu_0 - d_{k|cg}\dot{q}. \tag{42}$$

From equation (33), we know that

$$\dot{w} = \begin{bmatrix} Z_w & u_0 \end{bmatrix} \begin{bmatrix} w \\ q \end{bmatrix} + \begin{bmatrix} Z_{\delta_e} \end{bmatrix} \delta_e, \quad \text{and}$$
$$d_{k|cg}\dot{q} = d_{k|cg} \left(\begin{bmatrix} M_w + M_{\dot{w}}Z_w & M_q + M_{\dot{w}}u_0 \end{bmatrix} \begin{bmatrix} w \\ q \end{bmatrix} + \begin{bmatrix} M_{\delta_e} + M_{\dot{w}}Z_{\delta_e} \end{bmatrix} \delta_e \right).$$

Hence,

$$a_{kz} = \mathbf{C}_{kz} \begin{bmatrix} w \\ q \end{bmatrix} + \mathbf{D}_{kz}\delta_e, \tag{43}$$

where

$$\mathbf{C}_{kz} := \begin{bmatrix} -d_{k|cg}M_w + (-d_{k|cg}M_{\dot{w}} + 1)Z_w & -d_{k|cg}(M_q + M_{\dot{w}}u_0) \end{bmatrix}, \tag{44}$$
$$\mathbf{D}_{kz} := \begin{bmatrix} -d_{k|cg}M_{\delta_e} + (-d_{k|cg}M_{\dot{w}} + 1)Z_{\delta_e} \end{bmatrix}. \tag{45}$$

Similarly, the transfer function can be determined by $H_{kz}(s) = \mathbf{C}_{kz}(s\mathbf{I} - \mathbf{A}_z)^{-1}\mathbf{B}_z + \mathbf{D}_{kz}$. For the Boeing B-747 model with $u_0 = 180m/s$ and $d_{k|cg} = 30m$, the transfer function is

$$H_{kz}(s) = \frac{115.3(s^2 + 1.003s + 7.108)}{s^2 + 2.893s + 5.729}.$$

Hence, H_{kz} has no zeroes with positive real parts, which implies that the system exhibits minimum phase characteristics. On the other hand, the delay of the elevator response is assumed to be 0.1 seconds, which can be represented as a first-order transfer function and is given as

$$G_{ed}(s) = \frac{1}{0.1s + 1}.$$

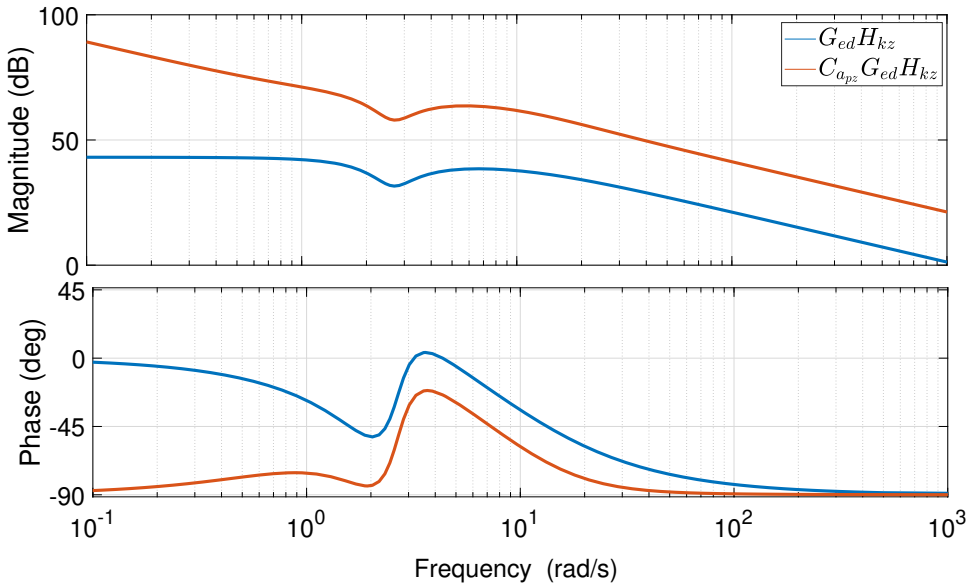

Fig. 4 Bode plot of the uncompensated (shown in blue) and compensated system (shown in orange).

By utilizing the Control System Designer tool in MATLAB and using the Bode plot method, we designed the compensator represented by the transfer function

$$C_{a_{pz}}(s) = 10\frac{(s+1)(s+20)}{s(s+10)}\,. \tag{46}$$

Figure 4 illustrates the bode plot of the transfer function $G_{ed}(s)H_{kz}(s)$ before and after applying the controller $C_{pz}(s)$. The blue curve represents the system without the controller, maintaining a stable gain across frequencies with a phase margin of 90.6 degrees at 1.15×10^3 rad/s, indicating robust stability. The orange curve includes the controller, enhancing the phase margin to 90 degrees at a higher frequency of 1.15×10^4 rad/s, illustrating effective control improvements at increased frequencies.

As a first step of the analysis, the tangential velocity profile during the zero-gravity maneuver is computed, with initial conditions set to $(V_0, \theta_0) = (180\text{ m/s}, \pi/4\text{ rad})$. The computed velocity profile, as illustrated in Figure 5, initiated at 180 m/s, decreased to approximately 127 m/s, and then returned to 180 m/s. For the detailed computation of the flight trajectory during the zero-gravity flight, including position, velocity, and path angle, refer to Appendix .A. In this context, the tangential velocity serves as the variable parameter for our linear aircraft model. A separate controller is assumed to manage the tangential acceleration effectively, allowing our focus to remain on the vertical acceleration control.

The controller's adaptability to different flight conditions was initially assessed by designing it for multiple Linear Time-Invariant (LTI) systems, each with a unique x^B-axis velocity (u) value. This controller configuration consistently demonstrated robust performance across the entire velocity spectrum, as evidenced in Figure 6. In the subsequent phase, the compensator was applied to a Linear Parameter-Varying (LPV) system. In this more complex scenario, the controller's response remained robust, effectively handling the system dynamics. The response of the LPV system, along with the corresponding elevator deflection, is depicted in Figure 7, highlighting the controller's versatility and capability in managing intricate dynamic challenges within this advanced modeling framework.

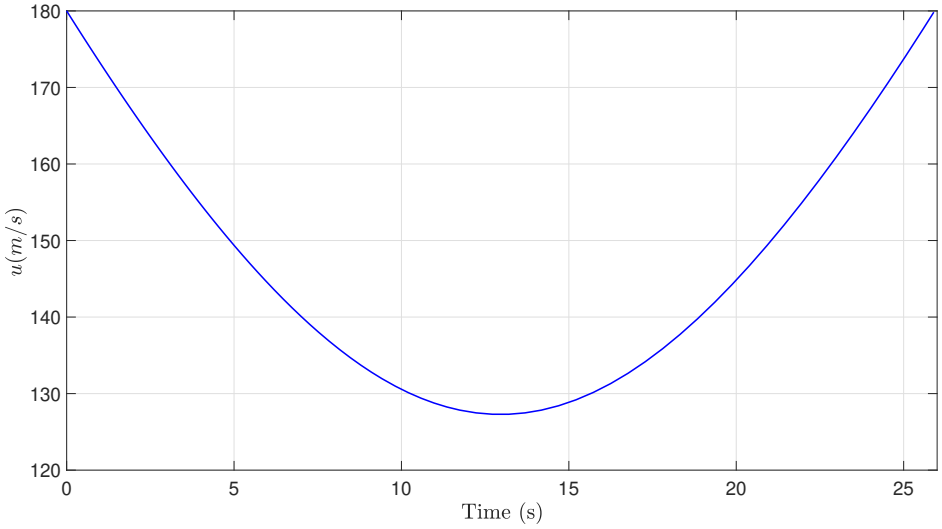

Fig. 5 Velocity profile for zero gravity flight with initial value $u_0 = 180m/s$.

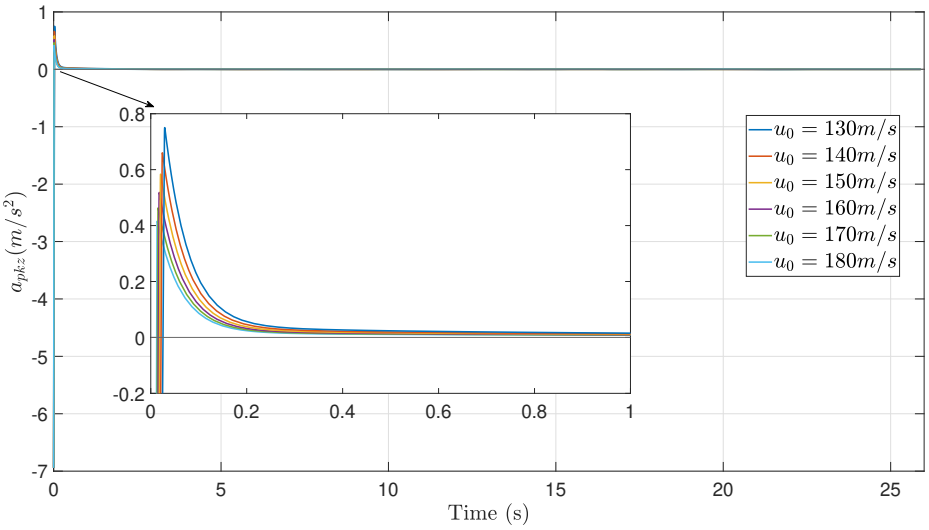

Fig. 6 LTI systems responses for zero gravity maneuver.

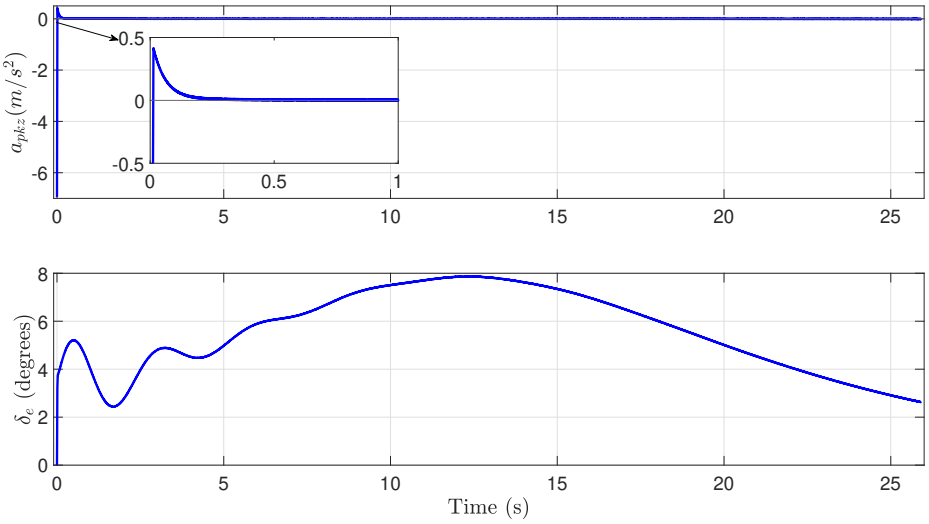

Fig. 7 LPV system response and elevator deflection for zero gravity maneuver.

VII. Tangential Acceleration Controller

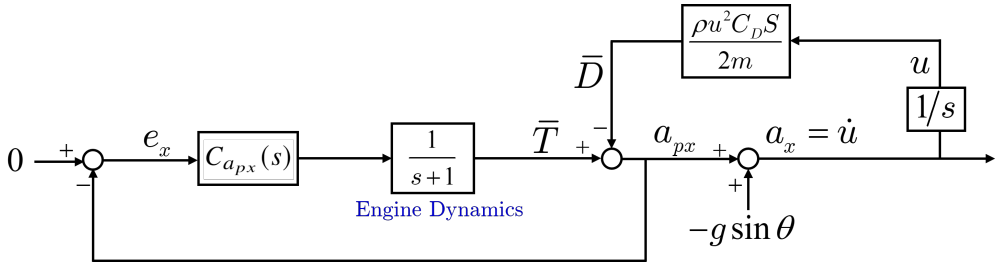

Fig. 8 Block diagram of the system used in designing the tangential acceleration controller.

In this section, we discuss the design of a flight controller for tangential acceleration. This controller is specifically engineered to manage tangential acceleration by effectively countering air resistance through appropriate thrust force adjustments. Figure 8 illustrates the configuration of the system used to design the controller. Two main assumptions have been made for the design of the controller:

- the angle of attack is very small, i.e., $\alpha \approx 0$, and
- the normal acceleration controller works perfectly.

By using the above two assumptions, equation (2) becomes

$$\Sigma F_x = T - D - W \sin\theta. \tag{47}$$

Moreover, the tangential acceleration of the CG can be approximated by the rate change of the tangential velocity, such as

$$a_x = \dot{u}. \tag{48}$$

Hence,

$$\dot{u} = \bar{T} - \bar{D} - g \sin\theta, \tag{49}$$

where $\bar{D}$ is the drag force normalized by the mass of the airplane. Furthermore, the tangential proper acceleration can be described as

$$a_{px} = \bar{T} - \bar{D}. \tag{50}$$

Thus, to achieve zero a_{px}, the thrust must compensate for the drag force, i.e., $T = D$. The drag force can be estimated, such as in Equation (5), where it is a function of the square of the velocity $D = 1/2\rho S C_D V^2$. Given that drag varies with speed and is challenging to measure or estimate accurately, our goal is to create a thrust control system capable of autonomously compensating for this uncertain drag. This system leverages the dynamic nature of aerodynamic forces encountered during parabolic flights to ensure effective drag rejection. References [28] and [18] propose using a controller with triple integral actions to reject the unknown drag that evolves quadratically with time. The designed controller is described as

$$C_{px} = 10\frac{(s+1)(s+0.4)(s+0.4)}{s^3}. \tag{51}$$

Figure 9 illustrates the system time response of acceleration of point k in x^B-axis and the thrust input during the zero gravity maneuver. It shows that the controller is capable of rejecting the drag force with a settling time of less than 3 seconds.

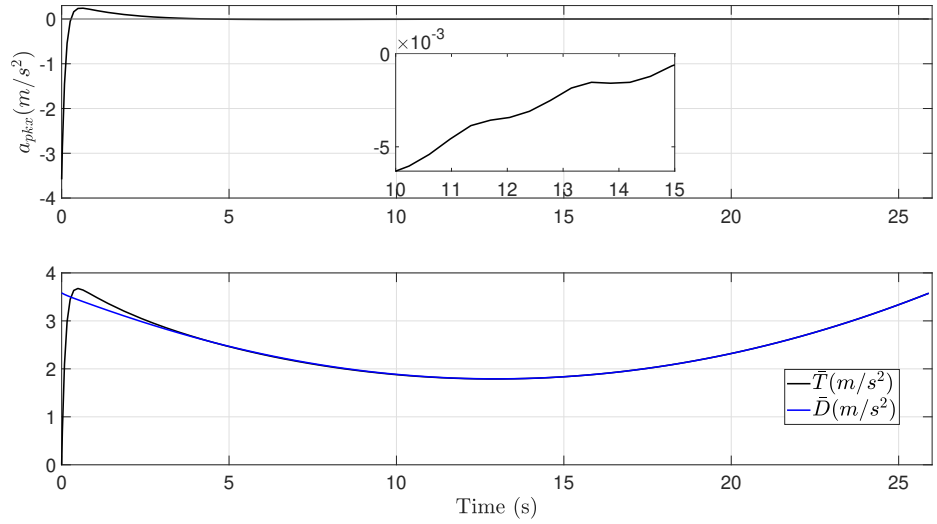

Fig. 9 The system time response of acceleration in x^B-axis and the thrust input during the zero gravity maneuver.

VIII. Simulation Results

The Boeing B-747 airplane is selected as a case study in this research to validate the proposed flight controller design. The data of the geometric, mass, and aerodynamic characteristics of Boeing B-747 can be found in [25]. The simulation setup, utilizing MATLAB Simulink [29], involves positioning an accelerometer within the cockpit, precisely aligned with the aircraft's x^B-axis. Following the independent design of the two controllers, we integrate them with the nonlinear model of the Boeing B-747. This integrated approach allows us to evaluate the controllers' robustness and performance thoroughly. Figure 10 illustrates the system time response of accelerations along x^B and z^B-axes and inputs during zero gravity flight. It indicates that throughout the maneuver, the system effectively avoids servo saturation, maintaining operational efficiency. Figure 11 shows a plot of the magnitude of the G levels. We can see that the system settles within 3.45 seconds and has a steady state average residual acceleration equal to $0.0022g$. The residual acceleration drops to values in the order of magnitude of 10^{-4} or less after about 13 seconds until the end of the maneuver. According to acceleration data of over 400 parabolic flights, typically, the optimal conditions for research in microgravity, referred to as the "sweet zone," last between 4 to 10 seconds on average with $\pm 0.01g$ residual acceleration [30]. Hence, the performance of the proposed flight controller shows that the system can maintain the duration of effective microgravity for about 22.4 seconds, which is significantly longer than the typical durations observed, potentially increasing the window for conducting scientific research under microgravity conditions.

Moreover, Figure 12 illustrates the longitudinal state variables of the aircraft during the zero gravity maneuver, demonstrating that they align with the anticipated profiles. The developed controller exhibits a satisfactory performance

across various partial gravity maneuvers, including those simulating lunar gravity. This is exemplified in Figures 13, 14, and 15, which display the system's time response and inputs, the G level, and state variables during a lunar gravity flight scenario. Mirroring the efficiency observed in zero-g flights, the system settles after 3.90 seconds with an average absolute error maintained at $0.0033g$.

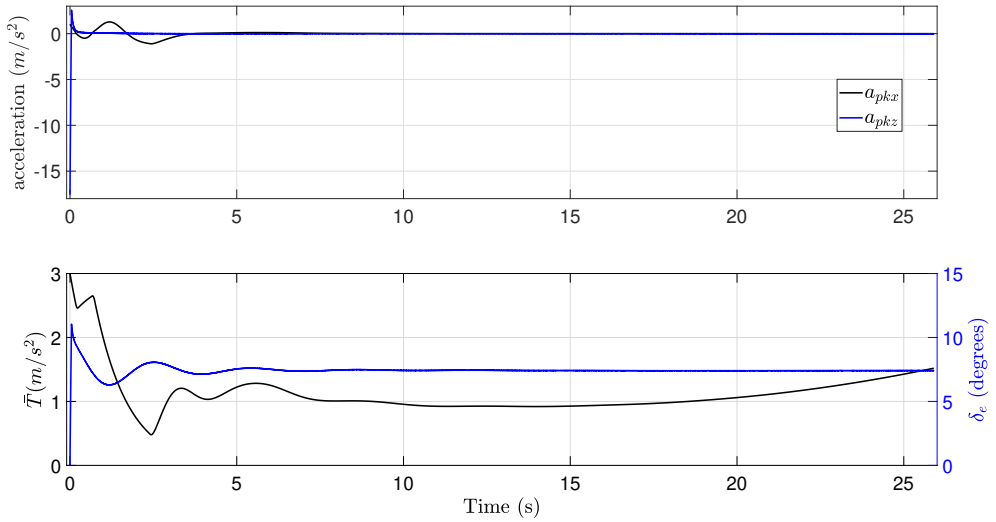

Fig. 10 The system time response of accelerations along x^B and z^B-axes during zero gravity flight.

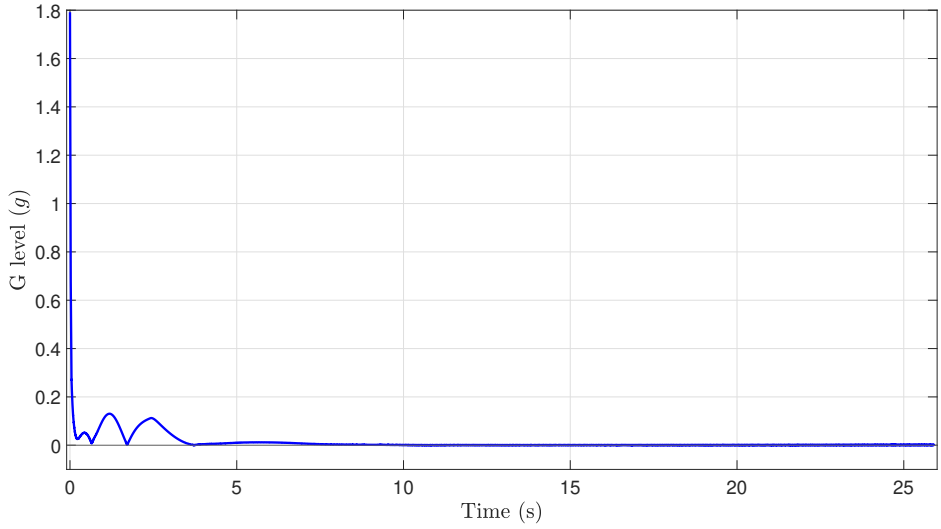

Fig. 11 The magnitude of G level during zero gravity flight.

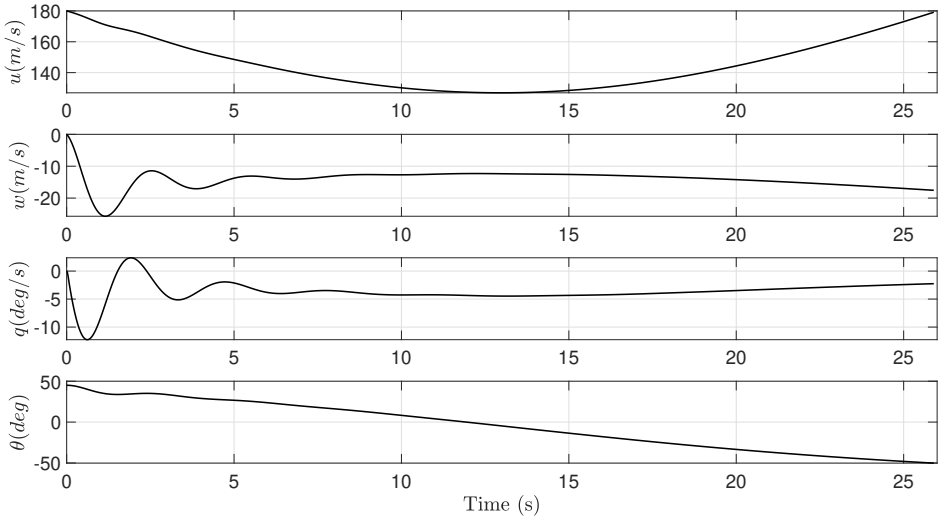

Fig. 12 State variables of the airplane during zero gravity flight.

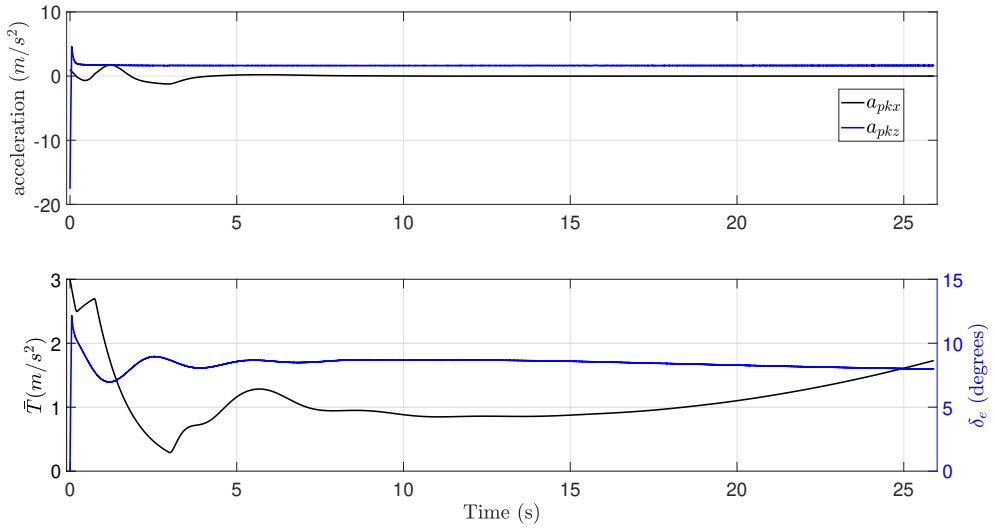

Fig. 13 The system time response of accelerations along x^B and z^B-axes and system inputs during moon gravity flight.

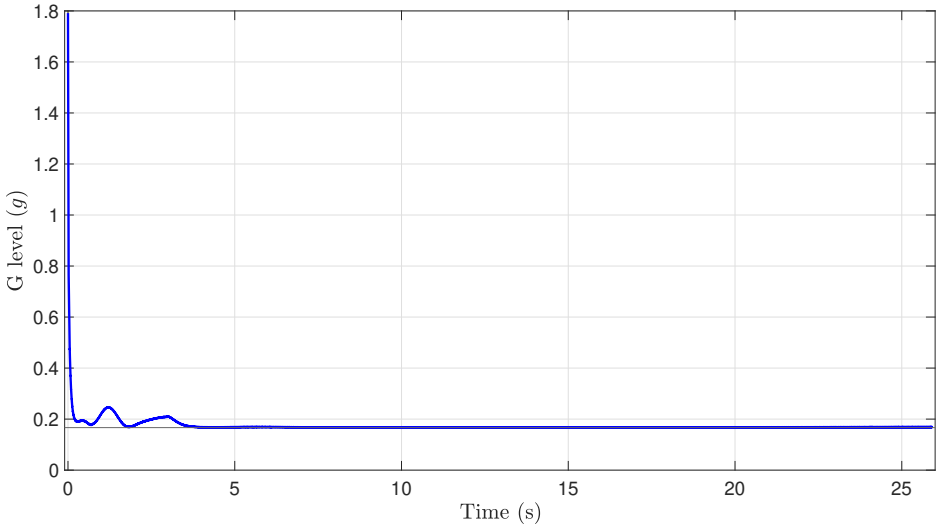

Fig. 14 The magnitude of G level during moon gravity flight.

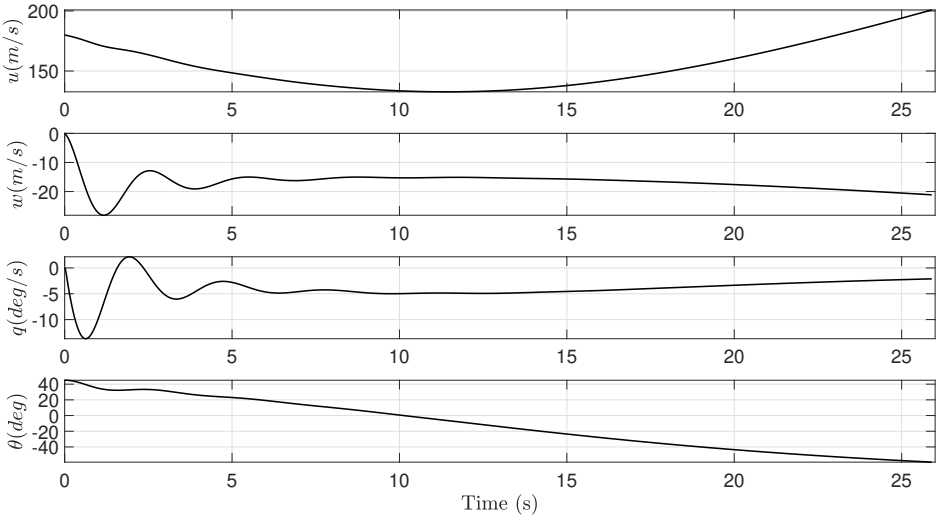

Fig. 15 State variables of the airplane during moon gravity flight.

A. Data Visualization in FlightGear

FlightGear is a free, open-source flight simulator first FlightGear, a free and open-source flight simulator, was first released in 1997 [31]. To enhance the understanding and intuition of reduced gravity flight, we visualized the flight maneuver using simulation data from Simulink. This was done through the FlightGear Preconfigured 6DoF Animation block within Simulink [32]. This specific block requires the aircraft's longitude and latitude, which can be derived from its velocities and orientations (roll, pitch, yaw) by applying navigation equations (52) and geodetic position computations (53).

$$\begin{aligned} \dot{x} &= V\cos\gamma = u\cos\theta + w\sin\theta \\ \dot{h} &= V\sin\gamma = u\sin\theta - w\cos\theta \end{aligned} \tag{52}$$

$$\dot{\phi} = \frac{V_N}{M+h}, \quad \dot{\lambda} = \frac{V_E}{(N+h)\cos\phi}, \tag{53}$$

where V_N and V_E are the geographic system North and East components of velocity in the inertial Earth frame $\mathcal{F}_E$, M and N denote the meridian and prime vertical radii of curvatures. In our case, V_N is equal to $\dot{x}$, and V_E is equal to zero because only longitudinal motion is considered. The screenshots illustrating the reduced gravity maneuver in FlightGear are presented in Figure 16.

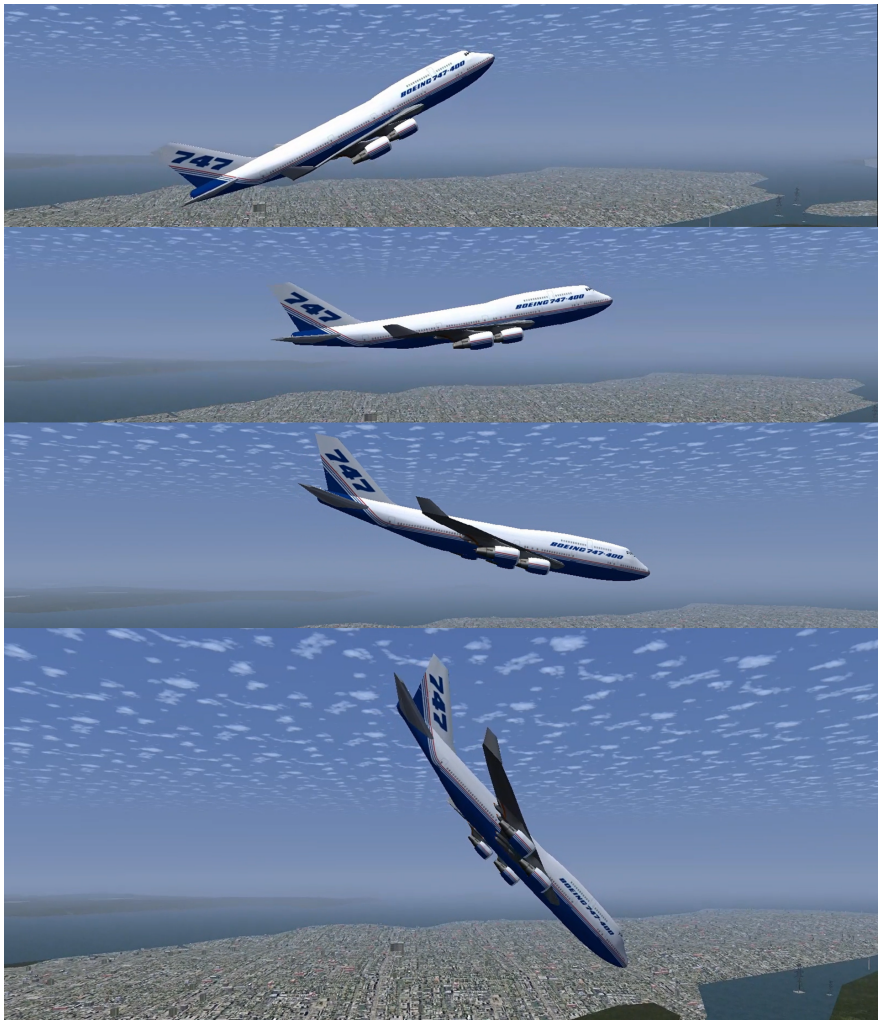

Fig. 16 Visualization of a microgravity maneuver in FlightGear (click here to watch the video).

IX. Conclusion

In conclusion, in this study, we design a flight control law for fixed-wing airplanes to conduct reduced gravity flights. The maneuver is assumed to happen in a 2D plane. Hence, two flight controllers are designed to control the two components of the acceleration to achieve the desired reduced gravity level. Moreover, the acceleration is used as the output for both controllers. Therefore, the only needed sensor to conduct the maneuver is an accelerometer. However, the transfer function from the elevator deflection to the normal acceleration of the airplane leads to a non-minimum

phase behavior of the system. Therefore, the sensor is placed in the cockpit to avoid the nonminimum phase issue. On the other hand, following earlier work, a controller with triple integral actions is designed to compensate for any air resistance in the tangential direction without the need for accurate measurements of those disturbances. Utilizing the aircraft's longitudinal model, both controllers are designed and then implemented on a nonlinear airplane model for reduced gravity flight simulations in MATLAB Simulink. These controllers demonstrate robustness across various levels of partial gravity. Furthermore, the FlightGear simulator enhances the visualization of these simulation results, effectively bridging the gap between theoretical control strategies and their practical, visual outcomes in a dynamic flight environment. The results show that the designed flight control law is capable of achieving and maintaining any reduced gravity level with accuracy and duration exceeding typical benchmarks, thus offering extended opportunities for more complex and varied experimental setups.

Future work to enhance the performance and reliability of the system includes addressing gust wind mitigation to improve stability and response under variable atmospheric conditions. Additionally, conducting flight tests will be important to validate the controller's effectiveness and safety in real-world scenarios. Furthermore, optimization of the airplane design will enable more efficient and precise control, ultimately leading to better performance in reduced gravity maneuvers. These combined efforts will significantly advance the capabilities and applications of the flight control system.

Appendix

A. Reduced Gravity Trajectory

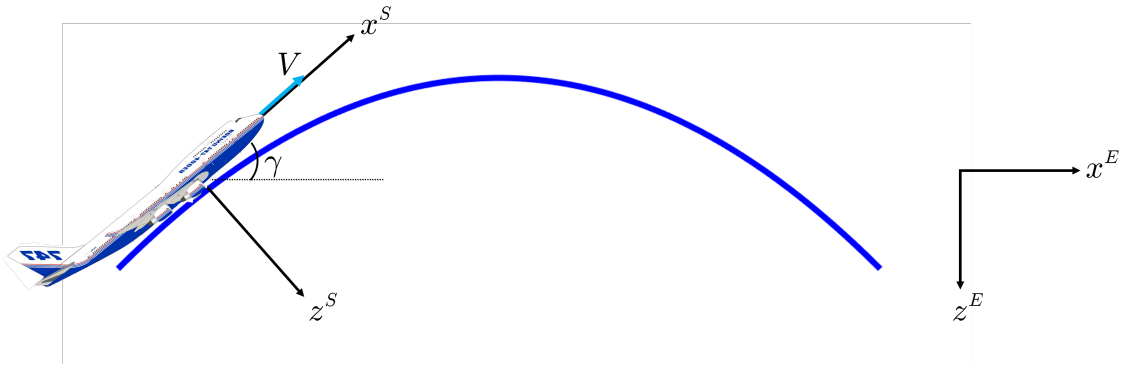

Fig. 17 Microgravity flight trajectory.

Figure 17 illustrates an aircraft executing a "parabolic" trajectory, a maneuver engineered to replicate the conditions of a microgravity environment within the airplane. Additionally, aircraft can achieve various levels of reduced gravity by following a specific trajectory for each desired gravity level. To calculate the flight trajectory that the aircraft needs to follow to conduct the reduced-gravity maneuver, a set of equations is derived to describe the motion in the inertial reference frame. The velocity components in this frame are given by

$$\dot{x} = V\cos\gamma, \tag{54}$$

$$\dot{z} = V\sin\gamma, \tag{55}$$

where $\dot{x}$ and $\dot{z}$ represent the rates of change of position in the horizontal and vertical directions, respectively, V is the magnitude of the velocity vector, and γ is the flight path angle relative to the horizontal.

The acceleration of the aircraft's center of gravity expressed in the Earth reference frame can be calculated using Euler's formula:

$$\mathbf{a} = \dot{\mathbf{V}} + \omega \times \mathbf{V}\,. \tag{56}$$

For a 2-D flight, the angular velocity vector ω can be represented as $\dot{\gamma}\mathbf{e_2}$, where $\mathbf{e_2}$ is the unit vector in the vertical direction. Assuming the velocity vector $\mathbf{V}$ is aligned with the x-axis of the body frame, we have $\mathbf{V} = V\mathbf{e_1}$, where $\mathbf{e_1}$ is

the unit vector in the horizontal direction. Hence, the acceleration vector **a** can be expressed as:

$$\mathbf{a} = \begin{bmatrix} \dot{V} \\ 0 \\ -\dot{\gamma}V \end{bmatrix}. \tag{57}$$

The goal of the reduced-gravity maneuver is to achieve and maintain some g-level by canceling forces acting along x^B and having some desired force along z^B, as discussed in Section III. Therefore, the equation for net force is:

$$m\mathbf{a} = m\mathbf{g} + F_{\text{non-gravitational}} = m \begin{bmatrix} -g\sin\gamma \\ 0 \\ g\cos\gamma \end{bmatrix} + m \begin{bmatrix} 0 \\ 0 \\ -\mu g \end{bmatrix}. \tag{58}$$

where m is the mass of the airplane, **g** is the gravitational acceleration vector, and $F_{\text{non-gravitational}}$ represents the non-gravitational forces acting on the aircraft.

By equating the components of acceleration and gravitational force vectors from equations (57) and (58), we obtain:

$$\dot{V} = -g\sin\gamma \tag{59}$$

$$\dot{\gamma} = \frac{(\mu - \cos\gamma)g}{V}. \tag{60}$$

These equations describe the rate of change of the aircraft's velocity and the rate of change of the flight path angle, respectively. By integrating equations (54), (55), (59), and (60), one can calculate the complete flight trajectory (V, γ, x, z) necessary for achieving the reduced-gravity condition.

Acknowledgments

This research was funded by the baseline support of King Abdullah University of Science and Technology. The author acknowledges support by a scholarship from the King Abdulaziz City for Science and Technology (KACST).

References

[1] Lundblad, N., Aveline, D. C., Balaz, A., Bentine, E., Bigelow, N. P., Boegel, P., Efremov, M. A., Gaaloul, N., Meister, M., Olshanii, M., et al., "Perspective on Quantum Bubbles in Microgravity," *arXiv preprint arXiv:2211.04804*, 2022.

[2] Rojas-Alva, U., and Jomaas, G., "A historical overview of experimental solid combustion research in microgravity," *Acta Astronautica*, 2022.

[3] Grimm, D., Wehland, M., Corydon, T. J., Richter, P., Prasad, B., Bauer, J., Egli, M., Kopp, S., Lebert, M., and Krüger, M., "The effects of microgravity on differentiation and cell growth in stem cells and cancer stem cells," *Stem Cells Translational Medicine*, Vol. 9, No. 8, 2020, pp. 882–894. https://doi.org/10.1002/sctm.20-0084, URL https://doi.org/10.1002/sctm.20-0084.

[4] Böhmer, M., and Schleiff, E., "Microgravity research in plants," *EMBO reports*, Vol. 20, No. 7, 2019, p. e48541. https://doi.org/https://doi.org/10.15252/embr.201948541, URL https://www.embopress.org/doi/abs/10.15252/embr.201948541.

[5] Rogers, M. J., Vogt, G. L., and Wargo, M. J., *Microgravity: A Teacher's Guide With Activities in Science, Mathematics, and Technology*, NASA, 1997.

[6] NASA, "What Is Microgravity?" , 2012. Available at https://www.nasa.gov/audience/forstudents/5-8/features/nasa-knows/what-is-microgravity-58.html.

[7] Pletser, V., *Gravity, Weight and Their Absence*, Springer, 2018. URL http://www.springer.com/series/8902.

[8] Pletser, V., Rouquette, S., Friedrich, U., Clervoy, J.-F., Gharib, T., Gai, F., and Mora, C., "European parabolic flight campaigns with Airbus ZERO-G: Looking back at the A300 and looking forward to the A310," *Advances in Space Research*, Vol. 56, No. 5, 2015, pp. 1003–1013. https://doi.org/https://doi.org/10.1016/j.asr.2015.05.022, URL https://www.sciencedirect.com/science/article/pii/S0273117715003622.

[9] Brigos, M., Perez-Poch, A., Alpiste, F., Torner, J., and Alonso, D. V. G., "Parabolic Flights with Single-Engine Aerobatic Aircraft: Flight Profile and a Computer Simulator for its Optimization," *Microgravity Science and Technology*, Vol. 26, 2014, pp. 229–239. https://doi.org/10.1007/s12217-014-9382-0.

[10] Pletser, V., Frischauf, N., Laufer, R., and Cohen, D., "Parabolic Flights with Gliders as an Innovative Low-Cost Platform for Microgravity and Hypergravity Research," *68th International Astronautical Congress (IAC)*, 2017.

[11] Hofmeister, P. G., and Blum, J., "Parabolic flights @ home: An unmanned air vehicle for short-duration low-gravity experiments," *Microgravity Science and Technology*, Vol. 23, 2011, pp. 191–197. https://doi.org/10.1007/s12217-010-9249-y.

[12] Siddhardha, K., "Microgravity Enabling Multirotors: Compact Like Drop Towers and Programmable Like Parabolic Flights," *Microgravity Science and Technology*, Vol. 33, 2021. https://doi.org/10.1007/s12217-021-09889-1.

[13] Afman, J.-P., Franklin, J., Mote, M. L., Gurriet, T., and Feron, E., "On the Design and Optimization of an Autonomous Microgravity Enabling Aerial Robot," *arXiv preprint*, 2016. URL http://arxiv.org/abs/1611.07650.

[14] "Zero-G," , 2 2022. URL https://www.gozerog.com/about-us/.

[15] "Take a gravity-free flight on board the Airbus A310 Zero G," , 4 2023. URL https://www.airzerog.com/.

[16] Amato, F., Ambrosino, G., Mattei, M., and Verde, L., "Design and robustness analysis of gain-scheduled control system for parabolic flight," *Journal of Guidance, Control, and Dynamics*, Vol. 19, 1996, pp. 430–437. https://doi.org/10.2514/3.21636.

[17] Hathaway, J. D., and Jacob, J. D., "Development of a microgravity generating flight mode for UAS," *AIAA Modeling and Simulation Technologies Conference*, 2016, p. 3219.

[18] Chen, Y.-H., and Feron, E., "Design of Longitudinal Control for Reduced-Gravity Atmospheric Flights," *AIAA SCITECH 2023 Forum*, 2023. https://doi.org/10.2514/6.2023-0218, URL https://arc.aiaa.org/doi/10.2514/6.2023-0218.

[19] Higashino, S., and Kozai, S., "Automatic Microgravity Flight System and Flight Testing Using a Small Unmanned Aerial Vehicle," , 2010.

[20] Afman, J. P., Feron, E., and Hauser, J., "Triple-Integral Control for Reduced-G Atmospheric Flight," *Proceedings of the American Control Conference*, Vol. 2018-June, 2018, pp. 392–397. https://doi.org/10.23919/ACC.2018.8431251.

[21] Kraeger, A. M., "Free-wing unmanned aerial vehicle as a microgravity facility," *Journal of Guidance, Control, and Dynamics*, Vol. 29, 2006, pp. 579–587. https://doi.org/10.2514/1.2274.

[22] Haber, F., and Haber, H., "Possible Methods of Producing the Gravity-free State for Medical Research," *Aero Medical Association*, 1950.

[23] "Parabolic manoeuvres," , 5 2020. URL https://www.esa.int/Education/Fly_Your_Thesis/Parabolic_manoeuvres.

[24] Karmali, F., and Shelhamer, M., "The dynamics of parabolic flight: Flight characteristics and passenger percepts," *Acta Astronautica*, Vol. 63, 2008, pp. 594–602. https://doi.org/10.1016/j.actaastro.2008.04.009.

[25] Nelson, R. C., et al., *Flight stability and automatic control*, Vol. 2, WCB/McGraw Hill New York, 1998.

[26] Slotine, J.-J. E., Li, W., et al., *Applied nonlinear control*, Vol. 199, Prentice hall Englewood Cliffs, NJ, 1991.

[27] Kim, S., and Horspool, K. R., "Nonlinear controller design for non-minimum phase flight system enhanced by adaptive elevator algorithm," *AIAA Scitech 2020 Forum*, 2020, p. 0603.

[28] Afman, J.-P., Feron, E., and Hauser, J., "Nonlinear Maneuver Regulation for Reduced-G Atmospheric Flight," *IEEE Conference on Decision and Control (CDC)*, 2018. URL https://ieeexplore.ieee.org/document/8618690.

[29] "Simulink - Simulation and Model-Based Design - MATLAB," , 2024. URL https://www.mathworks.com/help/simulink/.

[30] Lambot, T., and Ord, S. F., "Analysis of the quality of parabolic flight," *Next-Generation Suborbital Researchers Conference*, 2016.

[31] "FLIGHTGEAR FLIGHT SIMULATOR sophisticated, professional, open-source," , 1997. URL https://www.flightgear.org/.

[32] "FlightGear Preconfigured 6DoF Animation - Connect model to FlightGear flight simulator," , 2024. URL https://www.mathworks.com/help/aeroblks/flightgearpreconfigured6dofanimation.html.